PCCP

ROYAL SOCIETY OF CHEMISTRY

PAPER

View Article Online
View Journal | View Issue

Check for updates

Cite this: *Phys. Chem. Chem. Phys.*, 2020, **22**, 18536

Origin of photocatalytic activity enhancement in Pd/Pt-deposited anatase N-TiO_2 – experimental insights and DFT study of the (001) surface†

K. Batalović, *[ab] J. Radaković,[ab] N. Bundaleski,[ac] Z. Rakočević,[a] I. Pašti,[d] N. V. Skorodumova[ef] and C. M. Rangel[g]

Received 13th June 2020,
Accepted 22nd July 2020

DOI: 10.1039/d0cp03186k

rsc.li/pccp

In pursuit of the ideal photocatalyst, cheap and stable semiconductor TiO_2 is considered to be a good choice if one is able to reduce its band gap and decrease the recombination rate of charge carriers. The approach that offers such improvements for energy conversion applications is the modification of TiO_2 with nitrogen and noble metals. However, the origin of these improvements and possibilities for further design of single-atom catalysts are not always straightforward. To shed light on the atomic-scale picture, we modeled the nitrogen-doped (001) anatase TiO_2 surface as a support for palladium and platinum single-atom deposition. The thermodynamics of various synthesis routes for Pd/Pt deposition and nitrogen doping is considered based on density functional theory (DFT)-calculated energies, highlighting the effect of nitrogen doping on metal dimer formation and metal–support interaction. XPS analysis of the valence band of the modified TiO_2 nanocrystals, and the calculated charge transfer and electronic structure of single-atom catalysts supported on the (001) anatase TiO_2 surface provide an insight into modifications occurring in the valence zone of TiO_2 due to nitrogen doping and Pd/Pt deposition at the surface. DFT results also show that substitutional nitrogen doping significantly increases metal–support interaction, while interstitial nitrogen doping promotes only Pt–support interaction.

1. Introduction

Surface properties play a crucial role in the reactivity of nanomaterials. Aiming for the successful photocatalytic applications of nanosized semiconductors, one is obliged to understand, model and modify their surface according to the desired behavior. Control over surface properties, and consequently reactivity, is of significant interest for future applications, mainly in renewable energy[1,2] and environmental chemistry.[3]

TiO_2 is, due to its stability, low price, and good physicochemical characteristics, a material of the highest interest in semiconductor engineering. Especially, the anatase TiO_2 phase has the highest electron mobility in comparison to the rutile and brookite phases.[4] Numerous studies have been performed aiming to reduce the TiO_2 band gap and achieve wider utilization of the solar spectrum and thus improve its photocatalytic properties. A successful approach proved to be doping with non-metals,[5–7] doping with metals such as Pt,[8] or interfacing metals by deposition at the surface.[9–12] The Pt ion at the TiO_2 surface acts as a charge-generation center, producing free and trapped charges.[13,14] Density functional theory (DFT)+U study revealed that N-doping promotes dissociative water adsorption, leading to favorable adsorbate–substrate interactions and stabilization of OH groups at the TiO_2 surface.[15] Therefore, combined metal modification and non-metal doping is a good approach for catalyst tailoring.[16–18] This, however, should be treated carefully, since dopants introduced in the TiO_2 lattice can have states near the conduction band (CB), allowing the formation of mid-gaps that can accelerate electron–hole recombination rates and hinder photocatalytic performance.[19]

Given that photocatalytic activity is considerably affected by the exposed facets, non-metal doping, for band gap optimization,

[a] *"VINČA" Institute of Nuclear Sciences – National Institute of the Republic of Serbia, University of Belgrade, Belgrade, Serbia. E-mail: kciric@vin.bg.ac.rs*
[b] *Center of Excellence for Hydrogen and Renewable Energy CONVINCE, P.O. Box 522, Belgrade, 11001, Serbia*
[c] *Centre of Physics and Technologica Research, School of Science and Technology, Nova University of Lisbon, 2829-516 Caparica, Portugal*
[d] *University of Belgrade, Faculty of Physical Chemistry, Studentski trg 12-16, Belgrade, 11158, Serbia*
[e] *Department of Materials Science and Engineering, School of Industrial Engineering and Management, KTH-Royal Institute of Technology, Brinellvägen 23, Stockholm, 100 44, Sweden*
[f] *Department of Physics and Astronomy, Uppsala University, Box 516, 751 20 Uppsala, Sweden*
[g] *LNEG, National Laboratory for Energy and Geology, Paço do Lumiar 22, Lisbon, 1649-038, Portugal*

† Electronic supplementary information (ESI) available: Supplementary data 1: XRD pattern of N-doped TiO_2; supplementary data 2: XPS spectrum N-TiO_2: N 1s lines and fit; supplementary data 3: calculated Löwdin charges for studied surfaces. See DOI: 10.1039/d0cp03186k

combined with synthesis routes for facet selectivity, has been proposed in several studies.[4,7,20,21] Although the surface energy of the (001) anatase surface is larger than that of the (101) surface,[4] few experimental approaches exist to synthesize catalysts with the (001) facet exposed. For example, Zhang *et al.*[22] obtained Ca and N co-doped TiO_2 sheets with the (001) facet exposed through a one-step hydrothermal process. The higher surface energy of the (001) surface is, in general, related to better photocatalytic reactivity.[7]

Doping of surface sites is, in fact, functionalization of the TiO_2 surface, and such a modified surface plays a catalytic role in complex photo-induced reactions enabling advanced technological applications.[1,23] The growth of metal nanoparticles on a TiO_2 substrate has been widely studied; Pt nanoparticles on TiO_2 were encapsulated by Ti and O from the support, forming significantly anisotropic Pt@TiO_2 interfaces along different directions.[24] Cu clusters on TiO_2 were studied as promising candidates for methanol synthesis reactions.[25] Ag supported on titania has been found to be efficient in the reduction of harmful gases such as nitrogen oxides.[26] Lately, single-metal atom catalysts have been attracting attention as a way of obtaining targeted properties, while consuming significantly fewer resources.[27] Single-atom deposition on top of the N-TiO_2 surface can be regarded as a method for fine-tuning of charge states of adsorbed metals, and, in this case, understanding the behavior of TiO_2 as a support for metal deposition is also significant. For instance, in their work regarding Au and Ag deposition on TiO_2, Schlexer *et al.* showed how non-metal dopants stimulate charge transfer between the metal and oxide surface.[16]

Our earlier work[28] showed that nitrogen-doping of a nano-sized TiO_2 surface, combined with Pd or Pt deposition at the surface, generates unique properties of these materials, *e.g.* the combination of a suitable band gap (2.35 eV) and higher absorption in the visible light range as compared to N-doped TiO_2, which enable better utilization of visible light. In this article, we extend previous research by reporting the X-ray photoelectron spectroscopy (XPS) analysis of the electronic structure of the valence zone, which outlines the synergetic effect of noble metals and nitrogen at the TiO_2 surface. Photocatalytic hydrogen evolution from methanol solution using Pd or Pt@N-TiO_2 was also demonstrated in the work of Chiu *et al.*[29]

To study the origin of such improvements, and to understand the fundamental properties of Pd or Pt modified N-TiO_2, as well as the interaction between N, Pd, and Pt atoms and the support, we use DFT to model N-doping and deposition of noble metals (Pt and Pd) as single atoms. Deposition of two metal atoms and dimer formation on the (001) anatase surface are also addressed. The studied systems are a model of single atom catalysts (SACs), with catalytic performance highly dependent on the spatial configuration and the electronic states of the deposited metals that interact with the support. This interaction modifies the stability, dispersion, and the charge states of SACs, and the local electronic states of the support.[30] The DFT approach provides an atomic-level insight into the fundamental properties of materials, which can enable the understanding of material performances. Some examples include the achieved synthesis of anatase TiO_2 with the exposed (001) facets[22] for hydrogen generation from methanol or ethanol solutions, and ultimately water, or the design of TiO_2-based supported catalysts for proton-exchange membrane fuel cells.[10]

2. Experimental methods

Nitrogen-doped TiO_2 (N-TiO_2) was synthesized *via* a solvothermal method[31] using urea (Acros Organics, purity 99%) as a nitrogen source and titanium(IV) isopropoxide (Acros Organics, purity 98%) as a titanium source (resulting in the molar ratio N/Ti = 0.1). The final solution was evaporated to dryness in a steam bath, and subsequently heated at 400 °C for 4 hours in a furnace (Termolab Fornos electronics LDA). Palladium and platinum were deposited on the N-TiO_2 surface by ultra-violet reduction from chloride solutions, targeting a 0.10 wt% Pt loading (Pt/N-TiO_2) and 0.05 wt% Pd loading (Pd/N-TiO_2), using a photo-reactor with a 450 W Hg immersion lamp (ACE Glass Incorporated, NJ) and irradiation time of 60 min at a constant temperature (30–40 °C). The solution was filtered, dried and finally calcined at 440 °C for 1 h to obtain Pt, Pd/N-TiO_2 nanoparticles.

XPS analysis of the valence band (VB) was carried out in a SPECS customized ultra-high vacuum surface analysis system containing a PHOIBOS 100 spectrometer for energy analysis, a dual-anode Al/Ag monochromatic source and an electron flood gun. XPS spectra were obtained in fixed analyzer transmission mode using a monochromatic Al Kα line (photon energy of 1486.74 eV). Survey and high resolution spectra were obtained with the pass energy of 40 eV (energy step 0.5 eV) and 20 eV (energy step 0.1 eV), respectively. The position of the Ti $2p_{3/2}$ line, expected to be at 458.6 eV in the case of anatase,[32] was used as a binding energy reference for all samples.

3. Theoretical calculations

The effects of nitrogen doping and metal deposition on the (001) surface of anatase TiO_2 were studied using spin-unrestricted DFT-based calculations, with the Perdew–Burke–Ernzerhof general gradient approximation (PBE-GGA)[33] and a pseudopotential plane wave approach, as implemented in the Quantum ESPRESSO package.[34] Vanderbilt-type ultrasoft pseudopotentials were used, explicitly including the following valence states in the calculations: 3s, 3p, 3d, and 4s states for Ti, 2s and 2p states for O and N, 5d, 6s, and 6p states for Pt and 4d and 5s states for Pd. Plane waves were expanded using a kinetic energy cut-off of 30 Ry, while for charge density, a 16 times larger cut-off was adopted. An irreducible Brillouin zone was sampled using Monkhorst–Pack sampling[35] and a $2 \times 2 \times 1$ grid of *k*-points.

To correct the shortcomings of the GGA functional when addressing the electronic structure of the studied surfaces, the *U* value of 3 eV was applied to the 3d states of Ti, as it was not shown to significantly affect the ordering of vacancy and dopant states in the gap.[36] On the other hand, very large and unphysical *U* values ($U = 6$ eV) for the on-site correction of Ti 3d states were required to reproduce the experimental band gap;[23]

therefore, the value used in our work improves slightly the band gap given by GGA, and is also shown to be optimal for the study of metal deposition on a TiO_2 surface, giving satisfactory precision of total energy differences for these applications.[16,36] Additionally, doping energies calculated with and without U correction were compared, and aside from the energy shift when U is applied, no change in general trend is seen.

The anatase TiO_2 bulk structure was initially optimized, giving lattice parameters a = 3.816 Å and c = 9.513 Å, which are in agreement with the experimentally reported values (3.796 Å and 9.444 Å).[37] The (001) surface of TiO_2 was modeled using a (3 × 3) supercell, containing four Ti layers and twice as many O layers in a slab, with a 15 Å vacuum separating the surface slabs. A section of the relaxed (001) slab containing the model cell is shown in Fig. 1. The resulting model cell contains 96 atoms (32 Ti, 64 O), and it was relaxed with the two bottom Ti layers and corresponding O layers fixed at their bulk positions, until the forces acting on the atoms were less than 0.001 eV $Å^{-1}$ in any Cartesian direction.

According to the standard notation in the literature,[23] coordinately unsaturated surface Ti and O atoms were labeled Ti_{5c} and O_{2c}, respectively, while fully coordinated O atoms in the subsurface layer were labeled O_{3c}. Following the supercell relaxation, Ti_{5c}–O_{2c} surface bonds were found to be nonequivalent, with bond distances of 1.74 Å and 2.26 Å, in agreement with previous reports (1.8 Å and 2.2 Å).[23] The number of slab layers in the model cell was sufficient to assure consistency of the calculated surface energy for the (001) anatase surface (0.98 J m^{-2}) with the value of 1.01 J m^{-2} obtained by Liu *et al.*[38]

An identical relaxation procedure was applied while modeling the nitrogen doping and metal deposition on top of the relaxed (001) TiO_2 surface. Two types of nitrogen doping were simulated in our study, interstitial doping (N_{int}-TiO_2) and substitutional doping (N_{sub}-TiO_2). Interstitial doping was modeled by placing a N atom on the surface in plane with the other atoms, between the first and the second Ti layers, and between the second and the third layers. After relaxation of the supercells, the N atom was positioned above the surface, see Fig. 5a; regardless, we refer to this configuration as interstitial. For the substitutional doping, we addressed two cases, *i.e.* nitrogen substituting O_{3c} and O_{2c} atoms (see Fig. 1) in the surface layer. In the case of metal deposition on the nitrogen-doped TiO_2 surface, the most stable interstitial and substitutional N-TiO_2 surfaces were employed as the supports for metal atoms. This is a simplification of the correlated nitrogen–metal effect, but it was done with the aim to simulate the experimental procedure used in this work. However, some implications of other synthesis routes are discussed based on the total energy differences provided in Section 4.4. Deposition of Pt or Pd was modeled by adding metal atoms onto various surface sites next to nitrogen on the (001) surface – on top of Ti and at the bridge site. All structures were relaxed and optimized according to the procedure used for the starting slab. In addition, the deposition of metals away from the surface nitrogen was tested (labeled in text as next), as well as the deposition of metal atoms on top of the relaxed surface of the clean (pristine) (001) anatase TiO_2 surface. To model metal dimer formation at the surface during deposition, two metal atoms were placed next to each other at the surface, and the obtained structures were fully relaxed.

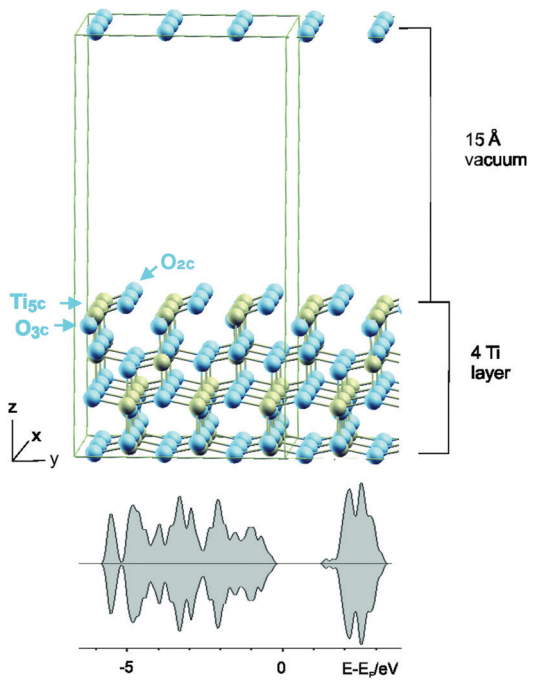

Fig. 1 Relaxed model of the (001) anatase TiO_2 slab (unit cell is framed); blue and gray spheres denote oxygen and titanium, respectively. At the bottom of the image, the resulting total density of states is shown.

4. Results and discussion

4.1. The motivation for follow-up research

Our earlier work[28] addressed Pd or Pt deposition at the surface of nanosized N-TiO_2, which proved to be an efficient catalyst in photocatalytic hydrogen production from ethanol. A wide range of applications of N-doped TiO_2 led to the development of many approaches, such as sputtering, ion implantation, pulse-laser deposition, sol–gel, oxidation of TiN, hydrothermal processing and NH_3 annealing[39,40] for N-TiO_2 synthesis. Also, various precursors were used, *e.g.* N-TiO_2 nanocatalysts with a homogeneous anatase structure were successfully synthesized through a microemulsion-hydrothermal method by using some organic compounds, such as triethylamine, urea, thiourea, and hydrazine hydrate (the optimal mole ratios of N to Ti for triethylamine, urea, thiourea, and hydrazine hydrate were 2, 1, 0.5, and 0.5, respectively).[41]

Having in mind this perspective, the approach we used for obtaining Pd, Pt/N-TiO_2 with a dominant anatase structure is just one possibility. However, the synthesis procedure and conditions for obtaining N-TiO_2 determine not only the dominant TiO_2 phase but also defect concentration and nitrogen position (substitutional and interstitial).[39,42] These structural variations lead to enhanced properties of the photocatalysts, but they also, given that they are a combination of many factors, hinder our understanding of the underlying interactions between nitrogen,

metals, and the TiO_2 surface. Our intention in this follow-up study was to understand the origin of the photocatalytic enhancement of nitrogen-doped metal-deposited anatase TiO_2, by looking at the atomic-scale picture of the TiO_2 surface based on the results of DFT calculations. In this work, earlier experimental findings regarding bonding and electronic structure[28] are viewed in correlation with the calculated thermodynamic and bonding properties. Also, additional XPS measurements of the valence band of the studied samples are done, given that the underlying structures of the VB and CB are straightforwardly obtained in the DFT calculations.

4.2. Experimental study of Pd, Pt surface modification and N-doping of anatase TiO_2 nanoparticles

Based on the X-ray diffraction (XRD) analysis (Supplementary data 1, ESI†), the studied materials have a dominant structure of the anatase phase, with a small percentage of the rutile phase (3.8%), and crystallite sizes of 12 ± 2 nm.[28] Our previous XPS study[28] also resolved the surface composition of the samples based on the intensities of characteristic photoelectron lines recorded in high resolution and the atomic sensitivity factors provided by the manufacturer of the XPS system. Relative elemental concentration of the atoms on the surface are: 0.4% nitrogen in N-TiO_2, 0.4% Pd in Pd/N-TiO_2 and 2.1% Pt in Pt/N-TiO_2. The majority of nitrogen is ascribed to interstitial doping, based on the evidence of N–O bond formation (67.3%), while some of the nitrogen is found to substitute the oxygen in the TiO_2 lattice (21.5%) (XPS spectrum shown in Supplementary data 2 (ESI†) and discussed in detail elsewhere[28]). Additionally, chemical states of the studied noble metals were addressed; as shown in Fig. 3, Pt is found to be present in a partially oxidized state. Three contributions to the Pt $4f_{7/2}$ line at 70.8 eV (49.1%), 72.5 eV (36.6%), and 74.7 eV (13.4%) were observed, giving evidence of metallic platinum, presumably in the Pt–Ti–O bond, and a small amount of PtO_2.[28]

The Pd $3d_{5/2}$ line situated at 336.6 eV has a unique contribution fully consistent with the PdO phase,[28] showing that all of the palladium found at the surface is in the Pd^{2+} form, see Fig. 2.

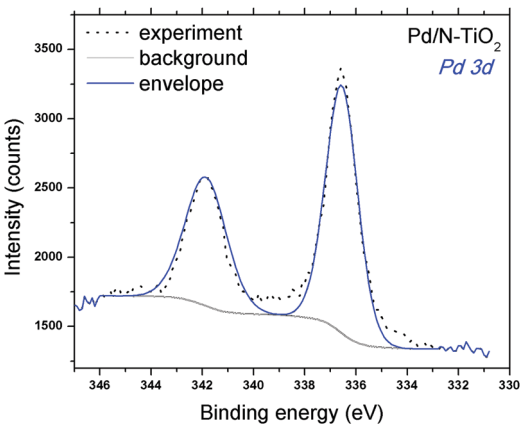

Fig. 2 XPS spectrum of the inelastic contribution of Ti 3s and Pt 4f lines from the Pt/N-TiO_2 sample (reproduced from ref. 28 with permission from the PCCP Owner Societies).

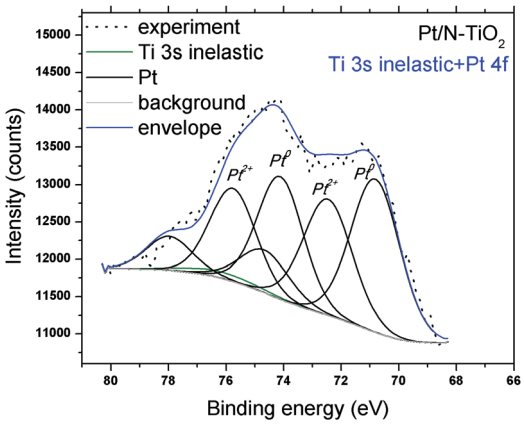

Fig. 3 Detailed XPS spectrum of the Pd 3d line from the Pd/N-TiO_2 sample (reproduced from ref. 28 with permission from the PCCP Owner Societies).

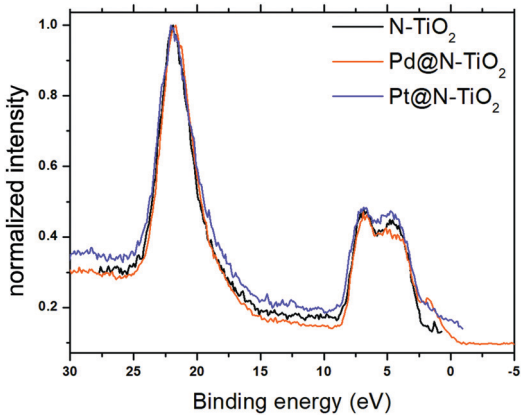

Fig. 4 XPS spectra of VB (intensity normalized to the maximum of the O 2s line) for N-TiO_2, Pd/N-TiO_2, and Pt/N-TiO_2, recorded with a pass energy of 20 eV (FAT 20 regime).

Valence bands of the reference material (N-TiO_2) and Pd- and Pt-loaded N-TiO_2 were recorded; Fig. 4 shows the normalized VB spectra. The position of the O 2s line at 21.8 eV overlaps for the three samples, justifying the usage of the Ti $2p_{3/2}$ line as a binding energy reference. The valence band shape is the result of two peaks at 8 eV and 6 eV, resulting from π and σ O 2p orbitals, respectively,[43] confirming the dominant anatase TiO_2 structure.

Based on the intersection of the valence band edge and background asymptotes, we find the top of the valence band of the reference sample to be around 2.2 eV below the Fermi level. Having in mind the XPS line broadening due to the non-uniform charging of the samples, we expected to find the VB edge at higher binding energies as compared to those of the theory[44] and UPS (ultraviolet photoelectron spectroscopy) experiments.[45] In the case of Pt- and Pd-loaded samples, the situation is significantly changed: the top of the VB moved toward higher energies, see Fig. 4. For Pd-deposition, a unique level inside the energy gap of the initial N-TiO_2 is detected above the VB top (shoulder at 1.8 eV). A similar effect, although

less pronounced, is seen in the case of Pt deposition, where the widening of the VB top is in the shape of an exponentially declining function.

4.3. Nitrogen doping and single-metal atom deposition on the (001) anatase TiO_2 surface – spatial configuration and energetics

We addressed both interstitial doping (N_{int}-TiO_2) and substitutional doping (N_{subs}-TiO_2) of the (001) anatase surface. The former one is of higher significance in relation to our experimental findings, given that previous research[28] demonstrated that, following the used synthesis procedure, the majority of nitrogen is relaxed into interstitial positions (see Supplementary data 2, ESI†).

The energy of interstitially doped nitrogen on the (001) TiO_2 surface is calculated with reference to N_2(g):

$$\Delta E(N_{int}) = E(N_{int}/TiO_2^{slab}) - 1/2E(N_2) - E(TiO_2^{slab}) \quad (1)$$

where the energy of the reconstructed surface is taken for the energy of TiO_2^{slab}.

The findings of Ortega *et al.* and Finazzi *et al.*, regarding the stability of nitrogen on the (101) anatase surface,[6,18] also indicate that the most stable structure is interstitially doped nitrogen on the surface of the TiO_2 slab. Based on the smallest value of the implantation energy for the (001) surface, the results obtained in our simulations coincide with the previously mentioned ones (sub-surface implantation energy is 2.32 eV larger). The relaxed N_{int}-TiO_2 slab is shown in Fig. 5a and the corresponding energetics is available in Table 1. Significant rearrangement of the surface structure is seen, with formation of a short N–O bond; the calculated N–O distance is 1.27 Å, which is in accordance with earlier reports (1.3–1.4 Å).[18]

The energy of nitrogen substituting oxygen on the (001) anatase TiO_2 surface, *i.e.* the substitution energy, is determined as:

$$\Delta E(N_{subs}) = E(TiO_{2-x}^{slab}N) - 1/2E(N_2) + 1/2E(O_2) - E(TiO_2^{slab}) \quad (2)$$

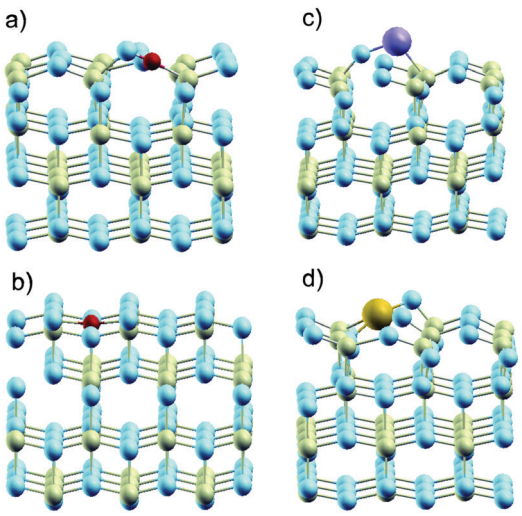

Fig. 5 Energetically preferred arrangements of the modified (001) anatase TiO_2 surface; (a) N_{int}-TiO_2, (b) N_{subs}-TiO_2, (c) Pt@TiO_2, and (d) Pd@TiO_2. Blue, gray and red small spheres denote oxygen, titanium, and nitrogen, while large purple and yellow spheres denote Pt and Pd, respectively.

The relaxed N_{subst}-TiO_2 structure is shown in Fig. 5b. The substitution of the O_{3c} atom is found to be more energetically favorable (ΔE = +4.60 eV) than substitution of the O_{2c} atom (ΔE = +4.77 eV) by 0.17 eV, which is in accordance with the threefold coordination of the N atom and corresponds to earlier reports for other anatase surfaces.[6,18] Earlier DFT studies showed that nitrogen sub-surface or bulk substitutions are slightly favored over surface substitutions.[18] However, to study the interaction of Pt and/or Pd with N atoms, we restrict our calculations to the most stable structures: interstitial nitrogen on the surface (N_{int}-TiO_2), and the more stable of the two surface substitutional cases – nitrogen substituting O_{3c} (N_{subs}-TiO_2). Both interstitial and substitutional nitrogen doping energies are positive, showing that nitrogen doping by molecular N_2(g) is thermodynamically unfavorable.

Table 1 also presents the calculated energies of metal deposition on the clean (reconstructed) TiO_2 surface, calculated as:

$$E(M_x) = E(M_x@TiO_2^{slab}) - E(TiO_2^{slab}) - xE(M); \quad x = 1, 2; \quad M = Pd, Pt \quad (3)$$

where E(M) is the energy of an isolated noble metal atom. The final structures of these two cases are shown in Fig. 5c and d. The relaxed structure of Pt doped (001) anatase TiO_2 is in agreement with the DFT study of Li *et al.*[11]

In addition to our results, Table 1 summarizes previously published energies of nitrogen doping and metal deposition on the (101) anatase TiO_2 surface, which is energetically the most favorable anatase TiO_2 surface. Although the previous DFT results and model surface sizes somewhat differ, a general trend regarding the energetics of nitrogen doping and platinum deposition is qualitatively consistent for the (001) and (101) surfaces. Positive nitrogen doping energies indicate an endothermic reaction for adsorption of nitrogen from the gas phase, which is expected given the high stability of molecular nitrogen.[18] Nevertheless, calculating the energy with reference to the standard state of nitrogen (N_2) provides an easy comparison of the nitrogen–surface interaction and is widely accepted in the literature. Synthetic routes use other nitrogen sources and external conditions in the synthesis, and the final nitrogen-doped slab is stable (negative energy).

Charge transfer for the clean (001) anatase TiO_2 surface and the N-doped surface is always from Pd to the support and from the support to Pt (Supplementary data 3, ESI,† see detailed

Table 1 Calculated (PBE-GGA) energies of nitrogen doping and energies of single metal atom deposition (ΔE) on the (001) anatase TiO_2 surface. Literature data regarding nitrogen doping and noble metal deposition on the (001) and (101) anatase TiO_2 surfaces are provided for comparison

	ΔE (eV)	
Dopant	(001) TiO_2	(101) TiO_2
N_{int}	2.07	2.71[18]
N_{subs}	4.60	4.92[18]
Pt	−3.49	−2.84[46]
	−2.93[8]	
Pd	−3.17	−0.39[47]
Au		−0.61[16]
Ag		−1.04[16]

Discussion of charge transfer in Section 4.6). Although charge transfer from metal to support is not typical, similar behavior to that of palladium is seen in the case of Au deposition on TiO_2.[18]

4.4. Structure and energetics of Pd and Pt deposition on the N-doped anatase (001) TiO_2 surface

After considering the mono-atomic deposition of N, Pt, or Pd on top of the clean (001) TiO_2 surface, a synergy of nitrogen doping and metal deposition on the surface is considered. In Table 2, we summarize the stabilities of Pt@N-TiO_2 and Pd@N-TiO_2 for both interstitially and substitutionally doped N-TiO_2. To illustrate the experimental case of metal deposition, the energy of M@N-TiO_2 is referenced to the energy of the corresponding N-TiO_2. Additionally, to study other possible doping/deposition strategies, the energy of M@N-TiO_2 is evaluated with respect to the energy of the metal-deposited (M@TiO_2) surface or clean TiO_2 surface.

In Table 2, we see the small energy differences calculated among various reactions in some of the discussed cases; therefore, other factors including geometry, kinetics or experimental conditions during synthesis might lead to different deposition priorities.[19]

By comparing the presented energies with energies of deposition on the clean (001) surface, we concluded that doping anatase surface with nitrogen significantly increases metal-support interaction, *i.e.* promotes platinum deposition. In comparison to the deposition on clean TiO_2, metal deposition energy is lower for substitutionally nitrogen-doped surface by 2.32 eV, and for interstitially nitrogen-doped by 0.97 eV. The same trend was shown for Au deposition alongside N-doped 101 anatase TiO_2 in the study by Ortega *et al.*[18] On the other hand, deposition energy of Pd on N_{int}-TiO_2 is similar to the deposition energy of Pd on clean TiO_2, while N_{subs}-TiO_2 promoted this action by lowering the deposition energy by 1.23 eV. These trends are further discussed based on the charge transfer in the next section. Looking at the synthesis strategies simultaneous nitrogen doping and metal deposition could be achieved from a thermodynamic point of view. Nitrogen doping of metal-modified TiO_2 surface from the gas phase is still thermodynamically unfavorable (positive doping energies), although in some cases much more feasible as compared to doping of clean TiO_2 surface – this is especially true for interstitial nitrogen doping of platinum-deposited surface (nitrogen implantation energy lowered from 2.07 to 0.75 eV).

In summary, doping the anatase surface with nitrogen lowers metal adsorption energy in the case of substitutional nitrogen doping, showing that such nitrogen implantation increases metal-support interaction for both metals. On the other hand, interstitial nitrogen doping promotes Pt-support interaction, while for Pd no significant change in deposition energy is seen. However, one must keep in mind that substitutional doping is much less favored than interstitial doping (Table 1).

4.5. Energetics of metal dimers on pristine and N-doped anatase (001) TiO_2 surface

Beside a single-atom surface deposition, understanding the growth of metal clusters is also valuable for catalytic applications, as it can lead to new mechanisms that accelerate the catalytic reaction.[48,49] On the other hand, for some applications, including single-atom heterogeneous catalysis, deposition of a single-atom is essential and clustering must be avoided.[50,51] To simulate the initial step of the small cluster formation process at the (001) anatase TiO_2 surface (represented by the deposition of two metal atoms) and quantify the probability of small metal cluster formation on nitrogen-doped (001) anatase TiO_2, we compare the energetics of a single metal atom deposition on the surface with the energetics of metal dimer deposition. Metal dimer deposition energy on the clean and N_{int}-doped (001) anatase TiO_2 surface is calculated by taking $x = 2$ in eqn (3), meaning that here we refer to the energy released upon deposition of two separate metal atoms next to each other to form a dimer on the surface as the metal dimer deposition energy. Results are presented in Table 3.

By comparing the energy released during the deposition of one (Table 1) and two metal atoms (Table 3) on the pristine (001) anatase TiO_2 surface, one can argue that clustering is probable in the case of Pt, due to a large energy release for the second atom deposition. The identical behavior for Pt deposition at the (101) anatase surface is shown in the work of Han *et al.*,[46] where they demonstrated the growth of small Pt clusters. Vittadini and Selloni showed, in a DFT study[47] of the interaction of small Au clusters (Au_n, n = 1–3) with a stoichiometric and reduced (101) TiO_2 surface, that gold clustering on the TiO_2 surface is also favored. However, in the latter case, this conclusion holds for the case of a low concentration of vacancies on reduced (101) TiO_2 as they serve as nucleation centrers.[47] In the case of Pd deposition on pristine TiO_2, N_{int}-TiO_2 and Pd@N_{int}-TiO_2, dimer

Table 2 Calculated reaction energy (ΔE) and difference of reaction energy and corresponding energy on clean TiO_2 ($\Delta E - \Delta E^{pristine}$) of (1) single-metal atom deposition on the (001) facet of nitrogen-doped TiO_2; (2) simultaneous procedure of metal deposition and nitrogen doping of the (001) anatase TiO_2 surface; (3) nitrogen doping of the metal deposited (001) TiO_2 surface

Type of reaction		N position	ΔE (eV)		$\Delta E - \Delta E^{pristine}$ (eV)	
			M = Pt	M = Pd	M = Pt	M = Pd
(1)	$M + N\text{-}TiO_2^{slab} \rightarrow M@N\text{-}TiO_2^{slab}$	N_{int}	−4.46	−3.03	−0.97	+0.14
		N_{subs}	−5.81	−4.40	−2.32	−1.23
((2)	$M + 1/2N_2 + TiO_2^{slab} \rightarrow M@N\text{-}TiO_2^{slab}$	N_{int}	−2.38	−0.96	—	—
		N_{subs}	−1.21	0.2	—	—
(3)	$1/2N_2 + M@TiO_2^{slab} \rightarrow M@N\text{-}TiO_2^{slab}$	N_{int}	0.83	2.22	−1.24	+0.15
		N_{subs}	2.28	2.90	−2.32	−1.70

Table 3 Calculated energy (ΔE) of (1) metal dimer deposition on clean (001) anatase TiO_2 surface; (2) metal dimer deposition on nitrogen-doped (001) anatase N_{int}-TiO_2 surface; (3) secondary metal deposition on single-metal deposited and N-doped (001) anatase surface ($M@N_{int}$-TiO_2). For N-doped surface, reaction energy is compared with the energy of same reaction on the clean surface ($\Delta E - \Delta E^{pristine}$)

		ΔE (eV)		$\Delta E - \Delta E^{pristine}$ (eV)	
		M = Pt	M = Pd	M = Pt	M = Pd
(1) Metal dimer on TiO_2	$2M + TiO_2^{slab} \rightarrow M_2@TiO_2^{slab}$	−8.20	−5.21		
(2) Metal dimer on N_{int}-doped TiO_2	$2M + N_{int}\text{-}TiO_2^{slab} \rightarrow M_2@N_{int}\text{-}TiO_2^{slab}$	−8.72	−6.23	−0.52	−1.02
(3) Metal deposition on $M@N_{int}$-doped TiO_2	$M + M@N_{int}\text{-}TiO_2^{slab} \rightarrow M_2@N_{int}\text{-}TiO_2^{slab}$	−4.26	−3.20	+0.45	−1.16

formation is energetically quite similar, ranging from −3.03 eV to −3.20 eV (Tables 1–3).

The calculated energy released upon deposition of a second Pt atom at N_{int}-TiO_2 (Table 3, the last row) is less compared to the energy released for the first atom (Table 2, the last row); however, it is larger than the deposition energy on the clean TiO_2. Based on the calculated values presented in the tables, the energy released upon single metal deposition, on the clean or modified TiO_2, follows the trend: $Pt@Pt/TiO_2 > Pt@N_{int}$-$TiO_2 > Pt@Pt/N_{int}$-$TiO_2 > Pt@TiO_2$ for platinum deposition, and $Pd@TiO_2 \approx Pd@N_{int}$-$TiO_2 \approx Pd@Pd/N_{int}$-$TiO_2 > Pd@Pd/TiO_2$ for palladium deposition.

Now, let us consider Pt and Pd deposition on the N-TiO_2 surface. If we start with very low concentrations, in the case of Pt, the most favorable adsorption site is the N-site. It is almost 1 eV more favorable than adsorption on the pristine surface (*i.e.* far from N, see Tables 2 and 3). So, single Pt atoms will initially deposit on N sites. If a higher Pt loading is considered, new Pt atoms arriving on the surface can choose between Pt@N-TiO_2 and free N-sites. The latter ones are energetically more favorable and also if the concentration of Pt@N-TiO_2 is still low, the probability of making a dimer is low. As the concentration increases further, Pt atoms previously adsorbed at N-sites will serve as nucleation centers for dimer formation and further growth of larger particles. Pt atoms will not favor pristine (001) terrace sites as the adsorption energy is much smaller compared to that of other configurations. So, in the case of a low concentration of Pt, single Pt atoms are likely to be anchored to N-sites at the surface. Now, let us consider the same scenario for Pd deposition. At a very low concentration of Pd, pristine (001) terrace sites are slightly more favored than N-sites (Tables 1 and 2). So, there should be basically no preference between available sites (the difference is only 0.14 eV) and at a low concentration of Pd, single Pd atoms should be adsorbed on anatase, which was, just recently, confirmed experimentally.[52] As one starts to increase the concentration of Pd, dimers will start to form. Dimer formation is, however, favored on N-sites, so these sites can be considered as the nucleation centers for larger Pd particles. Nevertheless, agglomeration will take place even if there is no nitrogen dopant, if the concentration increases over a certain limit.[52] When larger particles grow at high metal concentrations, one can consider that cohesive energy is released per atom and both Pd and Pt have high cohesive energies.

To summarize so far, nitrogen interstitial doping can, therefore, be seen as a way of additional stabilization of the single-atom surface deposition, when platinum concentrations are comparable with the concentration of surface nitrogen. For both Pt and Pd, a larger energy for dimer deposition is obtained at N_{int}-TiO_2 as compared to that at the clean TiO_2 surface, suggesting that when depositing metals in higher concentration, N-doped sites also serve as nucleation centers for dimer formation and possibly formation of larger metal clusters. However, in the case of Pd deposition, dimer formation is energetically the least favorable on the pristine TiO_2, while on the nitrogen-doped surface, no significant difference in deposition energy per atom is seen when depositing one or two atoms. Based on the obtained results, single atom dispersions of both Pt and Pd can be achieved on N-doped anatase (001) TiO_2, but in the case of platinum, doping plays the crucial role from the energetic point of view. However, the presence of surface N affects the electronic structure of both deposited metals, as shown below.

4.6. Electronic structure trends

The density of states (DOS) for mono- and di-atomic metal deposition on a clean (001) anatase TiO_2 surface is presented in Fig. 6. Deposited metals contribute with their electronic states mainly in the band gap energy range, either on top of the VB or, in some cases, the bottom of the CB. Having in mind that p-type impurities have their states mainly located near the top of the VB, while n-type impurities have their states near the CB edge, the DOS shown in Fig. 6 implies that even atoms of the same type will behave differently if surface clustering occurs. Given the targeted electronic structure for photocatalytic water splitting, to achieve overpotentials for both proton reduction and oxygen species oxidation (*i.e.* H_2 and O_2 evolution reactions), the occurrence of the additional states at the top of the VB is desirable. Adding one more metal atom to form a surface dimer reflects in extra electronic states and further narrowing of the band gap. In all cases, there is no polarization of charge on either metal or substrate atoms.

Doping the (001) surface with nitrogen introduces an empty N-2p state in the band gap, which is consistent with every studied N position (surface, subsurface…).[16] Some difference is observed between substitutional and interstitial nitrogen implantation; this is discussed for bulk doping in our previous work.[28] Given that the majority of surface nitrogen is in the form of interstitial nitrogen,[28] we further analyze the details of the electronic structure modifications resulting from a combined interstitial nitrogen doping and metal deposition. In agreement with other studies,[18] interstitial nitrogen introduces three N-p orbitals; one free above the Fermi energy. In Fig. 7, a detailed analysis of metal deposition and nitrogen-doping shows how Pd

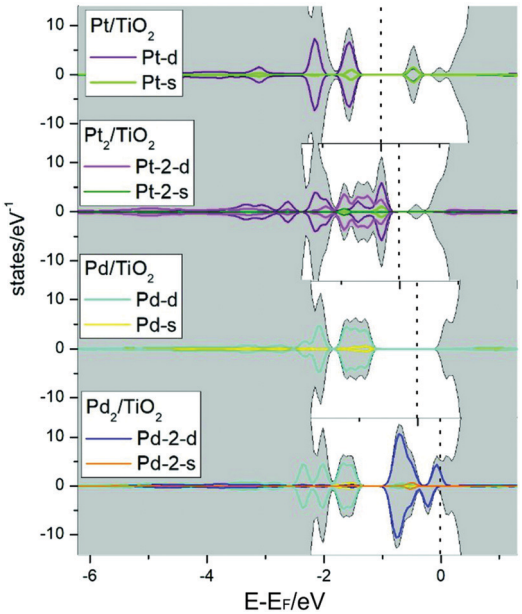

Fig. 6 Total density of states for the studied cases of single metal atoms and metal dimers on the clean TiO_2 surface (gray) with angular momentum-resolved contributions for metals (for the dimer cases, labels for the first atom correspond to the mono-doped case). Fermi energy is highlighted for each surface using a vertical dotted line.

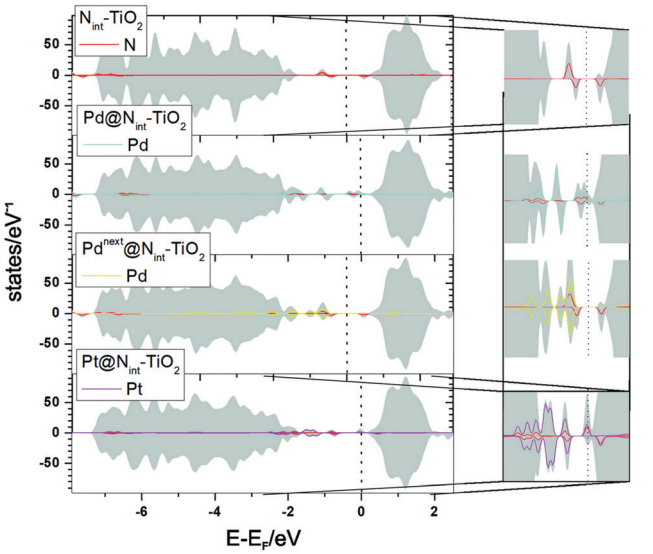

Fig. 7 Total density of states of single metal atoms deposited on the N_{int}-TiO_2 surface (gray) with metal-resolved contributions (red line corresponds to the DOS of nitrogen in all graphs); enlarged view of band gap region is shown for each case on the right; Fermi energy is highlighted for each surface using a vertical dotted line.

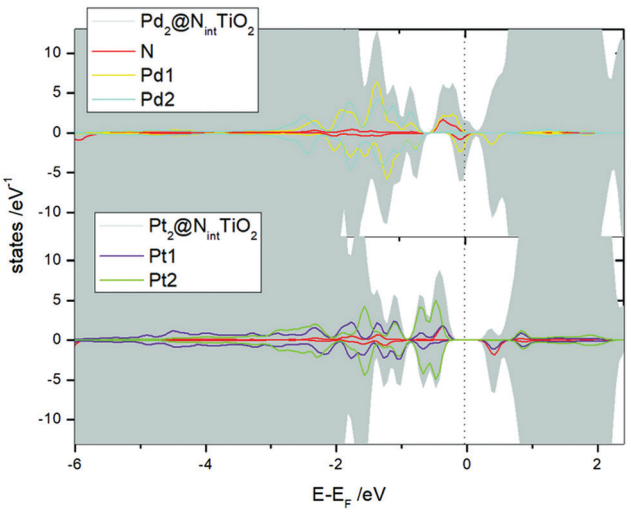

Fig. 8 Total density of states of metal dimers on the N_{int}-TiO_2 surface (gray) with metal-resolved contributions, and nitrogen contribution shown in red; Fermi energy is highlighted for each surface using a vertical dotted line.

and Pt states overlap with N states. Overall, this results in a continual population on top of the VB, as opposed to discrete dopant levels seen in the case of nitrogen doping. Additional charge is transferred to the N atom when Pd is deposited next to NO; this effect is seen as occupation of previously empty nitrogen states, comparing N_{int}-TiO_2 and Pd@N_{int}-TiO_2 in Fig. 7. This is also evident in the calculated charge transfer, presented in Fig. 9. Deposition further from N (labeled next) does not lead to significant coupling of nitrogen and metal states (Fig. 7, Pd^{next}@N_{int}-TiO_2).

On the other hand, Pt doping does not affect the occupation of empty N orbitals, given that platinum orbitals are lower in energy. This is the main difference in the behavior of palladium and platinum as surface modifiers; this trend is also present in the calculated charge transfer, shown in Fig. 9 and 10. Experiments by Pepin *et al.*[53] demonstrated the photocatalytic enhancement in the activity for photocatalytic reactions of acetaldehyde due to platinum deposition on TiO_2. As observed in the mentioned work, oxygen species adsorbed at the surface react with the photogenerated conduction band electrons captured by the Pt deposits, which prevents recombination of the photogenerated charge carriers. Having this in mind, nitrogen doping does not seem to significantly hinder photocatalytic enhancement given that Pt deposited at the surface of N-TiO_2 still has available empty electronic states.

Changes in electronic structure due to metal dimer deposition on N_{int}-TiO_2 are presented in Fig. 8. When depositing a Pd dimer on the surface of N_{int}-TiO_2, empty states of the second Pd atom shift above the Fermi energy, implying that if Pd clustering was achieved, it could serve as a center for electron transfer between the species involved, for example, in water splitting (proton reduction and the oxygen species oxidation). In the cases of both Pd- and Pt-dimers there is a strong overlap between the states of the two metal atoms and nitrogen, indicating chemical bonding, which can also be observed in the structures presented in Fig. 9. Clearly, the tuning of the electronic structure and the introduction of new states at the edges of the CB and VB could have a significant impact on the reactivity and catalytic activity of these systems. Recently, it was shown that very small Pt clusters with less than two atomic layers are efficient photoelectron collectors from

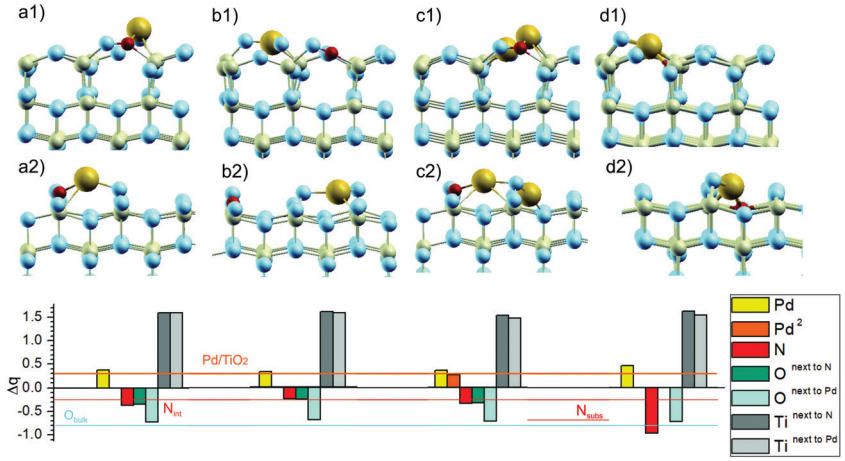

Fig. 9 (a) Pd@N_{int}-TiO_2, (b) Pd_{next}@N_{int}-TiO_2, (c) Pd_2@N_{int}-TiO_2, and (d) Pd@N_{subs}-TiO_2; (1) and (2) denote views from different slab sides; under each model cell is a corresponding Löwdin charge chart presenting the calculated charge with reference to the charge of an isolated atom (Δq).

TiO_2 bulk; by contrast, larger particles with more than two Pt layers are the active sites for hydrogen coupling to catalyze HER.[54]

Having in mind the energetics of single metal atom deposition discussed in Section 4.5, and the detailed DOS shown for metal deposition on clean and N-doped TiO_2, we can expect that additional structures formed on the top of the VB in metal-deposited samples seen in the XPS spectra (Fig. 4) are due to the interaction of Pt states with nitrogen (for Pt/N-TiO_2) or Pd states with the support and nitrogen (for Pd/N-TiO_2). Pt dimer formation also leads to additional states on top of the VB of TiO_2 and N-TiO_2 (see Fig. 6 and 8), consistent with the XPS spectra (Fig. 4). In our experimental study of Pt/N-TiO_2 nanocrystals,[28] we found 3 contributions to the Pt line, one of them corresponding to the significant contribution of metallic Pt (Fig. 2), *i.e.* evidence of Pt–Pt bond formation. Given that DFT results showed the highest energy released for Pt dimer formation on pristine TiO_2, we expect that clustering of Pt occurred on the TiO_2 support, and this might be due to the significantly smaller concentrations of surface nitrogen as compared to the surface Pt found in the studied samples.

The activity of the studied nanocatalysts was determined by the charge state of the metal atom. Charge state also provides an insight into the behavior of a metal during the synthesis; for example, stronger metal–support interactions can be used to avoid sintering during reaction that inactivates the metal. We discuss charge transfer based on the calculated Löwdin charges (valence charge states). The resulting charges presented here are referred to as the charge of isolated atoms, and a negative Löwdin charge indicates excess electrons compared to an isolated atom. For deep-lying Ti and O ions, calculated valence charge states amounted to +1.6 and −0.8, giving somewhat lower values as compared to the Bader charges[8] of +2.6 and −1.3 calculated based on atoms in molecules (AIM). The results obey the stoichiometry and correctly add up for bulk neutrality of the anatase TiO_2. In Fig. 9 and 10, these values are represented by the background lines as a reference for discussion of

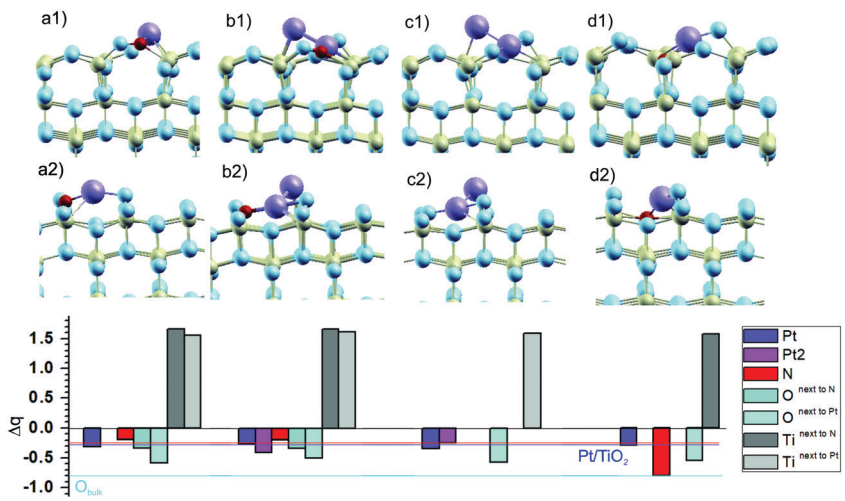

Fig. 10 (a) Pt@N_{int}-TiO_2, (b) Pt_2@N_{int}-TiO_2, (c) Pt_2@TiO_2, and (d)Pt@N_{subs}-TiO_2; (1) and (2) denote views from different slab sides; under each model cell is a corresponding Löwdin charge chart presenting the calculated charge with reference to the charge of an isolated atom (Δq).

charge transfer, which occurred due to doping. Lines representing the charge of mono-doped nitrogen, and single-atom deposited palladium and platinum are also shown. Calculated Löwdin charges for both substitutional nitrogen (−0.76) and interstitial nitrogen (−0.26) are in excellent agreement with the reported Bader charges (−0.89 and −0.30, respectively).[18]

Fig. 9 and 10 show relaxed slabs of the energetically most favorable structures for single atom and dimer metal deposition. Based on the charts presented in Fig. 9, we can highlight how co-doping with N and Pd affects charge transfer (Table S1 with the values for the studied cases given in the Supplementary data 3, ESI†).

In all studied cases, charge transfer is directed from palladium to the support, which is a less frequent case of charge transfer. This agrees with our experimental findings for anatase TiO_2 nanocrystals,[28] which point out that all of the deposited palladium is in the form of PdO. Unique contributions found for the Pd line in our XPS measurements (Fig. 3) indicate that all Pd atoms are deposited with the same charge transfer towards the matrix and any presence of metallic palladium is excluded. Having in mind the calculated dimer formation energies, we can conclude that our synthesis approach led to the deposition of small amounts of Pd, for which, as discussed in Section 4.5, dimer, and subsequently cluster, formation is not favored. If the metal is in proximity of the surface nitrogen, nitrogen further promotes the charge transfer from palladium. Thus, among the studied cases, the strongest metal–nitrogen interaction is observed when Pd is deposited on top of nitrogen, which is substituting for oxygen at the surface.

As can be seen in Fig. 10, Pt is negatively charged when deposited on the (001) anatase TiO_2 surface, which agrees with the results of Xia *et al.*[10] and experimental findings regarding a strong interaction with the support.[9] Lewera *et al.* found in their XPS study an increased electron density on Pt, which was reflected in the asymmetry of the Pt 4f XPS signal.[55]

5. Conclusions

Experimental XPS analysis of the valence band of a metal (Pd or Pt)-deposited surface of N-TiO_2 nanocrystals is compared to that of N-TiO_2, showing a shift of the top of the VB toward higher energy. For the Pd-modified sample, an additional level inside the energy gap of the initial N-TiO_2 is detected above the top of the valence zone (shoulder at 1.8 eV).

The structural and electronic properties of the (001) anatase TiO_2 surface, clean and doped with nitrogen, used as a support for Pd and Pt deposition, are studied using DFT+*U*. The thermodynamics of various synthesis routes for metal-deposited and nitrogen-doped (001) anatase TiO_2 surfaces is considered, highlighting the effect of nitrogen doping on metal clustering and metal–support interactions. According to the presented results, the nitrogen substituting oxygen (O_{3c}) significantly increases the metal–support interaction for both Pd and Pt, while interstitial nitrogen doping promotes only the Pt–support interaction. Analysis of diatomic deposition of noble metals on the top of the clean and N-doped surfaces indicates that from the energetic point of view, clustering can be avoided and single-atom deposition can be achieved for either metal on the N_{int}-TiO_2 surface when depositing in small concentrations.

Electronic structure analysis shows the overlapping of metal and nitrogen states, resulting in a continual population on the top of the VB, as opposed to discrete dopant levels seen in the case of nitrogen doping. Additional charge is transferred to the N atom when Pd is deposited next to NO at the surface, while Pt deposition does not influence the filling of empty N orbitals since Pt orbitals are lower in energy. This is the key difference in the behavior of Pd and Pt single-atoms as surface modifiers, and this general trend is present in the calculated charge transfer results. Clearly, the combination of TiO_2 doping with metal deposition provides an effective way for creation of new reactive centers and tuning the surface properties of the described materials. By a careful control of the metal deposition conditions, it seems that one can control the electronic structure of deposited atoms and the formation of metal aggregates. These results could be a guide for the further design of new TiO_2-based (photo)catalysts, while chemical and catalytic properties are yet to be carefully addressed.

Author contributions

The manuscript was written through contributions of all authors. All authors have given approval to the final version of the manuscript.

Abbreviations

VB	Valence band
CB	Conduction band
DFT	Density functional theory
DOS	Density of states
XPS	X-ray photoelectron spectroscopy
SAC	Single-atom catalyst

Conflicts of interest

There are no conflicts to declare.

Acknowledgements

The financial support for this study was provided through Projects no. 171001 and no. III 45005 financed by the Ministry of Education, Science and Technological Development of the Republic of Serbia, and through Portugal/Serbia bilateral Project no. 451-0301765/2014-09/03. Acknowledgments are also due to INIESC National Research Infrastructure in Solar Energy Concentration through project FCT_22113 (AAC 01/SAICT/2016), Portugal. The computations were performed on resources provided by the Swedish National Infrastructure for Computing (SNIC) at the High Performance Computing Center North (HPC2N) at Umeå University. Fig. 2 and 3, and Supplementary material 1 and 2 (ESI†), are

reproduced from ref. 28 with permission from the PCCP Owner Societies.

References

1 Y. Lan, Y. Lu and Z. Ren, Mini review on photocatalysis of titanium dioxide nanoparticles and their solar applications, *Nano Energy*, 2013, **2**, 1031–1045.

2 J. Li and N. Wu, Semiconductor-based photocatalysts and photoelectrochemical cells for solar fuel generation: a review, *Catal. Sci. Technol.*, 2015, **5**, 1360–1384.

3 F. Petronella, A. Truppi, C. Ingrosso, T. Placido, M. Striccoli, M. L. Curri, A. Agostiano and R. Comparelli, Nanocomposite materials for photocatalytic degradation of pollutants, *Catal. Today*, 2017, **281**, 85–100.

4 S. Ma, W. Song, B. Liu, W. Zhong, J. Deng, H. Zheng, J. Liu, X.-Q. Gong and Z. Zhao, Facet-dependent photocatalytic performance of TiO_2: A DFT study, *Appl. Catal., B*, 2016, **198**, 1–8.

5 C. Di Valentin, E. Finazzi, G. Pacchioni, A. Selloni, S. Livraghi, M. C. Paganini and E. Giamello, N-doped TiO_2: Theory and experiment, *Chem. Phys.*, 2007, **339**, 44–56.

6 E. Finazzi, C. di Valentine, A. Selloni and G. Pacchioni, First principles study on nitrogen doping at the anatase 101 surface, *J. Phys. Chem. C*, 2007, **111**, 9275–9282.

7 Y. Fan, C. Ma, B. Liu, H. Chen, L. Dong and Y. Yan, Nitrogen doped anatase TiO_2 sheets, *Mater. Sci. Semicond. Process.*, 2014, **27**, 47–50.

8 E. Mete, D. Uner, O. Gulseren and S. Ellialtroglu, Pt-incorporated anatase $TiO_2(001)$ surface for solar cell applications: First-principles density functional theory calculations, *Phys. Rev. B*, 2009, **79**, 125418.

9 J. Ohyama, A. Yamamoto, K. Teramura, T. Shishido and T. Tanaka, Modification of metal nanoparticles with TiO_2 and metal-support interaction in photodeposition, *ACS Catal.*, 2011, 187–191.

10 X. Xia, G. Jones, M. Sarwar, Q. Tang, I. Harkness and D. Thompsett, A. DFT study of Pt layer depositionon catalyst supports of titanium oxide, nitride and carbide, *J. Mater. Chem. A*, 2015, **3**, 245014.

11 Z. Li, X. Wang, L. Jia and X. Xing, Reduction of HCHO with OH^- on Pt loading anatase $TiO_2(001)$ surface: A DFT calculations, *Catal. Commun.*, 2017, **92**, 23–26.

12 Z. Li, A. A. Haidry, T. Plecenik, M. Vidis, B. Grancic, T. Roch, M. Gregor, P. Durina, Z. Yao and A. Plecenik, Influence of nanoscale TiO_2 film thickness on gas sensing properties of capacitor-like $Pt/TiO_2/Pt$ sensing structure, *Appl. Surf. Sci.*, 2020, **499**, 143909.

13 S. Kim, S.-J. Hwang and W. Choi, Visible light active platinum-ion-doped TiO_2 photocatalyst, *J. Phys. Chem. B*, 2005, **109**, 24260–24267.

14 E. Kowalska, H. Remita, C. Colbeau-Justin, J. Hupka and J. Belloni, Modification of titanium dioxide with platinum ions and clusters: application in photocatalysis, *J. Phys. Chem.*, 2008, **112**, 1124–1131.

15 S. Kenmoe and E. Spoh, Photooxidation of water on pristine, S- and N-Doped $TiO_2(001)$ nanotube surfaces: a DFT+*U* study, *J. Phys. Chem.*, 2019, **123**, 22691–22698.

16 P. Schlexer, A. R. Puigdollers and G. Pacchioni, Tuning the charge state of Au and Ag, *Phys. Chem. Chem. Phys.*, 2015, **17**, 22342–22360.

17 C. I. Fort, Zs. Pap, E. Indrea, L. Baia, V. Danciu and M. Popa, $Pt/N\text{-}TiO_2$ aerogel composites used for hydrogen production via photocatalysis process, *Catal. Lett.*, 2014, **144**, 1955–1961.

18 Y. Ortega, N. C. Hernandez, E. Mendez-Proupin, J. Graciani and J. F. Sanz, Nitrogen/gold codoping of the $TiO_2(101)$ anatase surface. A theoretical study based on DFT calculations, *Phys. Chem. Chem. Phys.*, 2011, **13**, 11340–11350.

19 W. Li., Influence of electronic structures of doped TiO_2 on their photocatalysis, *Phys. Status Solidi RRL*, 2015, **9**, 10–27.

20 S. Abu Bakar and C. Ribeiro, Prospective aspects of preferential {001} facets of N,S co-doped TiO_2 photocatalysts for visible-light-responsive photocatalytic activity, *RSC Adv.*, 2016, **6**, 89274–89287.

21 C. Li, C. Koenigsmann, W. Ding, B. Rudshteyn, K. R. Yang, K. P. Regan, S. J. Konezny, V. S. Batista, G. W. Brudvig, C. A. Schmuttenmaer and J.-H. Kim, Facet-dependent photoelectrochemical performance of TiO_2 nanostructures: an experimental and computationa study, *J. Am. Chem. Soc.*, 2015, **137**, 1520–1529.

22 J. Zhang, L. Qian, W. Fu, J. Xi and Z. Ji, Alkaline-earth metal Ca and N codoped TiO_2 with exposed 001 facets for enhancing visible light photocatalytic activity, *J. Am. Ceram. Soc.*, 2014, **97**, 2615–2622.

23 F. De Angelis, C. Di Valentin, S. Fantacci, A. Vittadini and A. Selloni, Theoretical Studies on Anatase and Less Common TiO_2 Phases: Bulk, Surfaces, and Nanomaterials, *Chem. Rev.*, 2014, **114**, 9708–9753.

24 M. Ahmadi, J. Timoshenko, F. Behafarid and B. Roldan Cuenya, Tuning the structure of Pt nanoparticles through support interactions: an in situ polarized X-ray absorption study coupled with atomistic simulations, *J. Phys. Chem. C*, 2019, **123**, 10666–10676.

25 H. Tao, Y. Li, X. Cai, H. Zhou, Y. Li, W. Lin, S. Huang, K. Ding, W. Chen and Y. Zhan, What is the best size of subnanometer copper clusters for CO_2 conversion to methanol at Cu/TiO_2 interfaces? a density functional theory study, *J. Phys. Chem. C*, 2019, **123**, 24118–24132.

26 A. B. Schvval, A. Juan and G. F. Cabeza, Theoretical study of the role of the interface of Ag_4 nanoclusters deposited on $TiO_2(110)$ and $TiO_2(101)$, *Appl. Surf. Sci.*, 2019, **490**, 343–351.

27 J. Liu, Catalysis by supported single metal atoms, *ACS Catal.*, 2017, **7**, 34–59.

28 K. Batalović, N. Bundaleski and J. Radaković, *et al.*, Modification of N-doped TiO_2 photocatalysts using noble metals (Pt, Pd) – A combined XPS and DFT study, *Phys. Chem. Chem. Phys.*, 2017, **19**, 7062–7071.

29 I. Chiu, S.-X. Lin, C.-T. Kao and R.-J. Wu, Promoting hydrogen production by loading PdO and Pt on $N\text{-}TiO_2$ under visible light, *Int. J. Hydrogen Energy*, 2014, **39**, 14574–14580.

30 S. Dong, B. Li, X. Cui, S. Tan and B. Wang, Photoresponses of supported Au single atoms on TiO_2(110) through the metal-induced gap states, *J. Phys. Chem. Lett.*, 2019, **10**, 4683–4691.
31 A. R. Gandhe and J. B. Fernandes, A simple method to synthetize visible light active N-doped anatase (TiO_2) photocatalyst, *Bull. Catal. Soc. India*, 2005, **4**, 131–134.
32 M. Biesinger, L. W. M. Lau, A. R. Gerson and R. St. C. Smart, Resolving surface chemical states in XPS analysis of first row transition metals, oxides and hydroxides: Sc, Ti, V, Cu and Zn, *Appl. Surf. Sci.*, 2010, **257**, 887–898.
33 J. P. Perdew, K. Burke and M. Ernzerhof, Generalized gradient approximation made simple, *Phys. Rev. Lett.*, 1996, **77**, 3865–3868.
34 P. Giannozzi, S. Baroni and N. Bonini, *et al.*, QUANTUM ESPRESSO: a modular and open-source software project for quantum simulations of materials, *J. Phys.: Condens. Matter.*, 2009, **21**, 395502.
35 H. J. Monkhorst and J. D. Pack, Special points for Brillouin-zone integrations, *Phys. Rev. B: Solid State*, 1976, **13**, 5188.
36 Z. Hu and H. Metiu, Choice of U for DFT+*U* calculations for titanium oxides, *J. Phys. Chem. C*, 2011, **115**, 5841–5845.
37 I. Djerdj and A. M. Tonejc, Structural investigations of nanocrystalline TiO_2 samples, *J. Alloys Compd.*, 2006, **413**, 159.
38 W. Liu, J.-G. Wang, W. Li, X. Guo, L. Lu, X. Lu, X. Feng, C. Liu and Z. Yang, A shortcut for evaluating activities of TiO_2 facets: water dissociative chemisorption on TiO_2-B (100) and (001), *Phys. Chem. Chem. Phys.*, 2010, **12**, 8721–8727.
39 X. Fang, Z. Zhang, Q. Chen, H. Ji and X. Gao, Dependence of nitrogen doping on TiO_2 precursor annealed under NH_3 flow, *J. Solid State Chem.*, 2007, **180**(4), 1325–1332, DOI: 10.1016/j.jssc.2007.02.010.
40 M. Sathish, B. Viswanathan, R. P. Viswanath and C. S. Gopinath, Synthesis, Characterization, Electronic Structure, and Photocatalytic Activity of Nitrogen-Doped TiO_2 Nanocatalyst, *Chem. Mater.*, 2005, **17**, 6349–6353.
41 Y. Cong, J. Zhang, F. Chen and M. Anpo, Synthesis and Characterization of Nitrogen-Doped TiO_2 Nanophotocatalyst with High Visible Light Activity, *J. Phys. Chem. C*, 2007, **111**(19), 6976–6982.
42 J. Wang, D. N. Tafen, J. P. Lewis, Z. Hong, A. Manivannan, M. Zhi and N. Wu, Origin of Photocatalytic Activity of Nitrogen-Doped TiO_2 Nanobelts, *J. Am. Chem. Soc.*, 2009, **131**, 12290–12297.
43 V. Pfifer, P. Erhart and S. Li, *et al.*, Energy Band Alignment between Anatase and Rutile TiO_2, *J. Phys. Chem. Lett.*, 2013, **4**, 4182–4187.
44 D. O. Scanlon, C. W. Dunnill and J. Buckeridge, *et al.*, Band alignment of rutile and anatase TiO_2, *Nat. Mater.*, 2013, **12**, 798–801.
45 A. Orendorz, J. Wüsten, C. Ziegler and H. Gnaser, Photoelectron spectroscopy of nanocrystalline anatase TiO_2 films, *Appl. Surf. Sci.*, 2005, **525**, 85–88.
46 Y. Han, C.-J. Liu and Q. Ge, Interaction of Pt Clusters with the Anatase TiO_2(101) Surface: A First Principles Study, *J. Phys. Chem. B*, 2006, **110**, 7463–7472.
47 A. Vittadini and A. Selloni, Small gold clusters on stoichiometric and defected TiO_2 anatase (101) and their interaction with CO: A density functional study, *J. Chem. Phys.*, 2002, **117**, 353.
48 M. Klein, J. Nadolna, A. Gołąbiewska, P. ŁMazierski, T. Klimczuk, H. Remita and A. Zaleska-Medynska, The effect of metal cluster deposition route on structure and photocatalytic activity of mono- and bimetallic nanoparticles supported on TiO_2 by radiolytic method, *Appl. Surf. Sci.*, 2016, **378**, 37–48.
49 Y. Watanabe, Atomically precise cluster catalysis towards quantum controlled catalysts, *Sci. Technol. Adv. Mater.*, 2014, **15**, 063501.
50 E. Fako, Z. Łodziana and N. López, Comparative single atom heterogeneous catalysts (SAHCs) on different platforms: A theoretical approach, *Catal.: Sci. Technol.*, 2017, **7**, 4285–4293.
51 J. Liu, Catalysis by Supported Single Metal Atoms, *ACS Catal.*, 2017, **7**, 34–59.
52 F. Yang, S. Ding, H. Song and N. Yan, *Sci. China Mater.*, 2020, **63**, 982–992.
53 P. A. Pepin, J. D. Lee, A. C. Foucher, C. B. Murray, E. A. Stach and J. M. Vohs, *J. Phys. Chem. C*, 2019, **123**, 10477–10486.
54 D. Wang, Z.-P. Liu and W.-M. Yang, *ACS Catal.*, 2018, **8**, 7270–7278.
55 A. Lewera, L. Timperman, A. Roguska and N. Alonso-Vante, *J. Phys. Chem. C*, 2011, **115**, 20153–20159.